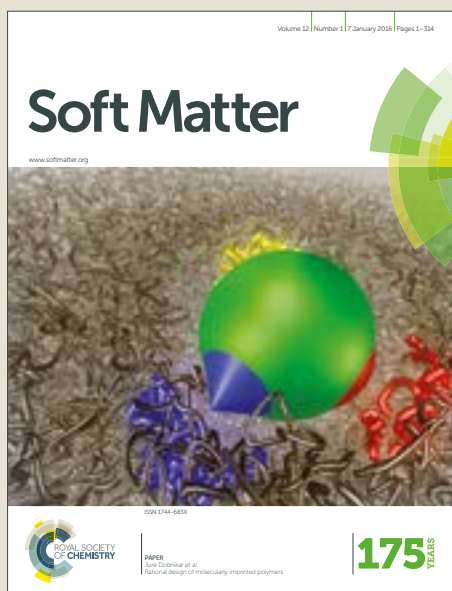


Soft Matter

Accepted Manuscript



This article can be cited before page numbers have been issued, to do this please use: Z. Tan, M. Yang and M. Ripoll, *Soft Matter*, 2017, DOI: 10.1039/C7SM01436H.



This is an Accepted Manuscript, which has been through the Royal Society of Chemistry peer review process and has been accepted for publication.

Accepted Manuscripts are published online shortly after acceptance, before technical editing, formatting and proof reading. Using this free service, authors can make their results available to the community, in citable form, before we publish the edited article. We will replace this Accepted Manuscript with the edited and formatted Advance Article as soon as it is available.

You can find more information about Accepted Manuscripts in the [author guidelines](#).

Please note that technical editing may introduce minor changes to the text and/or graphics, which may alter content. The journal's standard [Terms & Conditions](#) and the ethical guidelines, outlined in our [author and reviewer resource centre](#), still apply. In no event shall the Royal Society of Chemistry be held responsible for any errors or omissions in this Accepted Manuscript or any consequences arising from the use of any information it contains.

Cite this: DOI: 10.1039/xxxxxxxxxx

Anisotropic thermophoresis

Zihan Tan,^{*a} Mingcheng Yang,^{*b,c} and Marisol Ripoll^{*a}

Received Date

Accepted Date

DOI: 10.1039/xxxxxxxxxx

www.rsc.org/journalname

Colloidal migration in temperature gradient is referred to as thermophoresis. In contrast to particles with spherical shape, we show that elongated colloids may have a thermophoretic response that varies with the colloid orientation. Remarkably, this can translate into a non-vanishing thermophoretic force in the direction perpendicular to the temperature gradient. Oppositely to the friction force, the thermophoretic force of a rod oriented with the temperature gradient can be larger or smaller than when oriented perpendicular to it. The precise anisotropic thermophoretic behavior clearly depends on the colloidal rod aspect ratio, and also on its surface details, which provides an interesting tunability to the devices constructed based on this principle. By means of mesoscale hydrodynamic simulations, we characterize this effect for different types of rod-like colloids.

1 Introduction

The migration of particles in liquid environments with the presence of a temperature gradient was first described in the XIX century^{1,2} and it is generally known as thermal diffusion or Soret effect. The study of the Soret effect in liquid mixtures is usually referred to as *thermodiffusion*³. In these mixtures, all relevant particles sizes are similar and within the nanometer scale. The same physical principle applied to colloids is typically referred to as *thermophoresis*^{4,5}. Colloids can have sizes up to the micrometer scale and the surrounding solvent particles can be orders of magnitude smaller. Several factors are known to importantly influence the thermodiffusive behavior of these systems like the colloid size, mass, average temperature, concentration^{3,4}. In fluid mixtures the effect of the particle moment of inertia has been extensively studied^{6–8}, concluding that increased moment of inertia facilitates migration. Rodlike colloids have been experimentally investigated^{9,10} and characterized as a function of their electrostatic interactions. However, no systematic study has been yet done to investigate the thermophoretic properties of colloids as a function of their shape.

Most colloids show thermophobic behavior (average migration to the cold areas), although thermophilic colloids have also been frequently reported^{11,12}. In both cases, the colloid migration is characterized by a unique value of the so-called *thermal diffusion*

factor which, by convection, is positive for thermophobic colloids and negative for thermophilic. The sign and the value of the thermodiffusion factor is determined by the colloid size and properties of the colloid solvent interactions, and it can be modified or even reversed for example by changing average temperature, concentration, pH or solvent composition. But the question that arises is how is the thermophoretic behavior of elongated particles. A valuable and interesting parallelism can be made here between thermophoretic and friction forces. An elongated object moving in a fluid along its axis is known to experience frictional force γ_{\parallel} , which is typically much smaller than the friction experienced by the same rod moving perpendicular to its axis γ_{\perp} . This is a well-know fact, which in the case of a shish-kebab model of adjacent beads has been calculated to be $\gamma_{\perp} = 2\gamma_{\parallel}$ for aspect ratios larger than 20¹³. It is therefore intuitive, that an elongated object with its axis aligned with a temperature gradient, will not have the same thermophoretic response as when the axis is perpendicular to the gradient. Hence and in contrast to colloids with spherical symmetry, colloids with an anisotropic shape should be characterized by two or more thermal diffusion factors, which is the main concept of the *anisotropic thermophoresis*¹⁴. The corresponding effect was already predicted for elongated particles in gases, where the propulsion of particles aligned with the gradient was expected to be larger than that of particles perpendicular to the temperature gradient^{15,16}. The effect for colloids in liquid solutions is therefore still to be explored.

Practical applications of thermophoresis have developed over several decades and are currently in a significant expansion stage. Some relevant examples are crude oil characterization¹⁷, separation techniques¹⁸, strong components accumulation in prebiotic conditions^{19,20}, the precise characterization of proteins, for which thermophoresis can even distinguish between different

^a Theoretical Soft-Matter and Biophysics, Institute of Complex Systems, Forschungszentrum Jülich, 52425 Jülich, Germany. E-mail: z.tan@fz-juelich.de; m.ripoll@fz-juelich.de

^b Beijing National Laboratory for Condensed Matter Physics and Key Laboratory of Soft Matter Physics, Institute of Physics, Chinese Academy of Sciences, Beijing 100190, China. E-mail: mcyang@iphy.ac.cn

^c University of Chinese Academy of Sciences, Beijing 100049, China

binding states²¹; also various application in microfluidics^{22,23}, or the fabrication of synthetic microswimmers^{24–26}. The traditional versatility of thermophoresis is therefore importantly increased by considering different shaped objects.

In this work we investigate the anisotropic thermophoretic properties of colloidal rods by means of hydrodynamic computer simulations. We study the dependence of the thermophoretic forces for moving rods and for fixed rods at different orientations, with various aspect ratios and surface properties. The anisotropic effect can for example be reversed by changing the surface rugosity, which can be understood in terms of the associated temperature properties of the fluid in the vicinity of the colloid. Interestingly, this anisotropy can induce a thermophoretic effect non-aligned with the temperature gradient. This contribution to the thermophoretic force perpendicular to the temperature gradient has already shown to be the basic mechanism that allows the construction of thermophoretic turbines, which move in the presence of an external temperature gradient¹⁴. Other promising applications are not yet explored, but are certainly to be expected, and are specially promising in microfluidic devices where significantly large and well-localized temperature gradients can be generated and precisely controlled in time and space. Applications of anisotropic thermophoresis in the presence of external temperature gradients offer then the possibility of engineering devices able to harvest waste heat energy.

2 Simulation method

In order to be able to bridge the time and length scales of the colloidal rods and the surrounding solvent particles, a hybrid description of the suspension is employed. The solvent is simulated by an efficient technique known as multiparticle-collision dynamics (MPC)^{27–29}, while the colloidal rod is described with a Molecular Dynamics simulation model. In MPC, the solvent is represented by N point particles whose dynamics takes place in two sequential steps. One is the streaming step, at which all point particles move ballistically for a certain collision time h . In the collision step, particles are grouped into cubic collision cells of size a , where particles interchange momentum by performing a rotation by a certain angle α of the particle velocity relative to the corresponding cell center of mass velocity. MPC accounts for thermal fluctuations, and conserves energy and linear momentum both globally and locally^{30–32} by construction. Angular momentum is not conserved for this MPC implementation^{33,34}. However, recent work has provided evidence that angular momentum conservation in MPC fluid does not influence the hydrodynamics of phoretic flows³⁵. Simulations are performed with an average of $\rho = 10$ particles per collision cell, the collision time step $h = 0.1$, the rotation angle $\alpha = 130^\circ$, and the average temperature of the solvent $k_B \bar{T} = 1$. These numbers determine the fluid transport properties, such that the diffusion coefficient $D_s = 0.05$, the kinematic viscosity $\nu = 0.87$, or the thermal diffusivity $\kappa_T = 0.15$ ^{28,30,36–41}. The resulting Prandtl number, $Pr = \nu/\kappa_T = 5.8$, is really very close to that of various liquids such as water. The related Schmidt number, $Sc = \nu/D_s = 17$, is smaller than that of water, but shows that the propagation of momentum is faster than that of mass, namely collisional transport dominates

as in the case of liquid. The MPC method has largely shown to be a very efficient approach to simulate liquids with hydrodynamic interactions^{42,43}. In the following, all quantities are expressed in terms of the MPC units, where the units of length, mass and energy are separately imposed as a , m and $k_B \bar{T}$, such that the time unit is $(ma^2/k_B \bar{T})^{1/2}$. The temperature gradient is applied in the z direction with a boundary thermostat^{43–45}, ensuring that heat conduction is correctly accounted for.

The rod is constructed with the “shish-kebab” model built by N connected beads in a linear disposition as shown in Fig. 1. The excluded volume interactions between colloid and solvent are performed via MD with Lennard-Jones (LJ) type potentials^{46,47}

$$U_k(r) = \begin{cases} \infty; & r \leq \Delta \\ 4\epsilon \left[\left(\frac{d}{2(r-\Delta)} \right)^{2n} - \left(\frac{d}{2(r-\Delta)} \right)^n \right] + C; & \Delta < r < r_c \\ 0; & r_c \leq r \end{cases} \quad (1)$$

Here r is the distance between the bead center and the fluid particle, ϵ refers to the potential intensity, d to the bead diameter, and n is a positive integer describing the potential stiffness. The parameter Δ refers to a potential displacement, which we fixed as $\Delta = 0$ unless specified. The repulsive or attractive LJ potentials are obtained by considering $c = 1/4$ or $c = 0$ respectively, together with the adequate cutoff distance r_c . The repulsive and attractive potentials with stiffness $n = 6$ will be denoted as $r6$ and $a6$ respectively, and similar for other n values. The bead diameter is taken as $d = 4a$, and $\epsilon = k_B \bar{T}$. The mass of each bead is chosen such that the rod is neutrally buoyant, although results are not really depending on this value. The equations of motion of the beads and interacting fluid are integrated with a velocity-Verlet MD algorithm. The rod length L is given by $L = d + (N - 1)l$, such

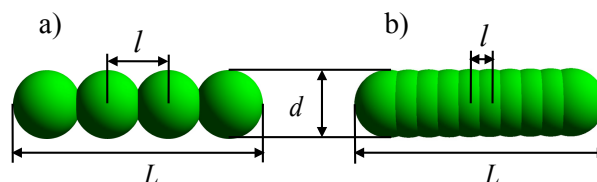


Fig. 1 Sketch of the “shish-kebab” model of a colloidal rod of aspect ratio $L/d = 3.7$ with variable number of beads N , and variable inter-bead separation l . (a) “Rough” rod with $N = 4$ beads and $l = 0.9d$. (b) “Smooth” rod with $N = 10$ beads and $l = 0.3d$.

that the aspect ratio L/d can be fixed for more than one combination of N and l . Besides the particular solvent-bead potential, the rod surface properties are going to be determined by the inter-bead separation, which we characterize with l/d , the rugosity parameter. As can be seen in Fig. 1, a rough rod is obtained when $l \simeq d$, while a smooth rod is obtained when $l \ll d$. In order to prevent the penetration of the fluid inside the rod, the maximum value of the rugosity parameter we employ is $l/d = 0.9$. We consider a three-dimensional box with periodic boundary conditions changing from 3 to 4 times the rod length L . Two types of simulations are performed. Simulations with fixed rods only need the colloid solvent interactions to be specified. Simulation with freely rotating rods and fixed central of mass, in which the rod motion

is additionally accounted with rigid body dynamics⁴⁸.

3 Results

The migration of a particle in a temperature gradient is driven by the thermophoretic force \mathbf{F}_T ^{49–51}. This force arises from the interactions between the particle and the surrounding inhomogeneous fluid environment. In the case of spherically symmetric colloids, this force is characterized by a unique value of the so-called *thermodiffusion factor*, α_T , as

$$\mathbf{F}_T = -\alpha_T k_B \nabla T, \quad (2)$$

with k_B the Boltzmann constant, and ∇T the temperature gradient. There is though no reason to expect that a unique factor would still describe the thermophoretic behavior of a non-spherically symmetric particle. A straightforward generalization can be written in terms of the *thermodiffusion tensor* Λ_T as

$$\mathbf{F}_T = -\Lambda_T \cdot \nabla T. \quad (3)$$

In a very general case, colloids with arbitrary shape and arbitrary surface properties can be defined by a symmetric tensor with independent coefficients. Of particular interest is the case of an homogeneous colloidal rod with cylindrical symmetry. In this case, two independent coefficients are expected to be enough to determine the thermodiffusion tensor as

$$\Lambda_T = \alpha_{T,\parallel} \hat{\mathbf{u}} \hat{\mathbf{u}} + \alpha_{T,\perp} (\hat{\mathbf{I}} - \hat{\mathbf{u}} \hat{\mathbf{u}}), \quad (4)$$

with $\hat{\mathbf{u}}$ the unit vector of long axis of rod. Here $\alpha_{T,\parallel}$ is the thermodiffusion factor of the long rod axis, or equivalently the thermophoretic factor that characterizes a rod with the long axis aligned with the temperature gradient, as displayed in Fig. 2a. Reciprocally, $\alpha_{T,\perp}$ is the thermodiffusion factor of the short rod axis, or of a rod with the long axis oriented perpendicular to the temperature gradient (see Fig. 2b).

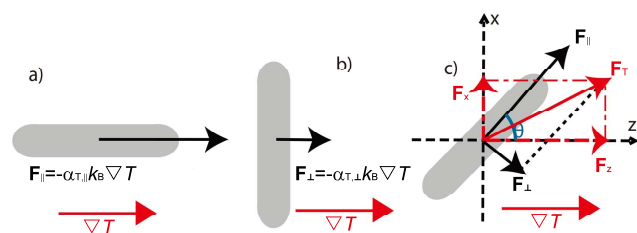


Fig. 2 Sketch of the thermophoretic force of a colloidal rod fixed with different orientations with respect to the temperature gradient: a) parallel, b) perpendicular, c) with an arbitrary θ angle.

3.1 Linear decomposition of the thermophoretic force

The thermophoretic force acting on a rod with arbitrary orientation can be determined by the linear superposition of the two components with orthogonal thermodiffusion factors $\mathbf{F}_T = \mathbf{F}_{\parallel} + \mathbf{F}_{\perp}$. The temperature gradients along the long and short axis are respectively $\nabla T_{\parallel} = \cos\theta \nabla T$ and $\nabla T_{\perp} = \sin\theta \nabla T$, with θ the angle between the particle long axis and the temperature gradient,

as displayed in Fig. 2c. The total force can then be expressed in terms of its components, parallel and perpendicular to the temperature gradient $\mathbf{F}_T = \mathbf{F}_{\parallel} + \mathbf{F}_{\perp}$ as,

$$\mathbf{F}_{\parallel} = -(\alpha_{T,\perp} \sin^2 \theta + \alpha_{T,\parallel} \cos^2 \theta) k_B \nabla T, \quad (5)$$

$$\mathbf{F}_{\perp} = (\alpha_{T,\perp} - \alpha_{T,\parallel}) \sin \theta \cos \theta k_B |\nabla T| \mathbf{n}_x \quad (6)$$

where \mathbf{n}_x is the unit vector perpendicular to ∇T . Equation (6) comes as a straightforward result of the tensorial character of the thermodiffusion tensor in Eq. (3), and strikingly implies that a non-vanishing thermophoretic force exists in the direction perpendicular to the temperature gradient. This force can in fact be easily measured in our simulations as shown in Fig. 3, such that it could also be measured experimentally^{52,53}. The measured force perpendicular to the temperature gradient is clearly non-vanishing, and it increases linearly with the applied temperature gradient, as expected from Eq. (6). This nicely confirms the tensorial character of the thermophoretic effect for objects without spherical symmetry.

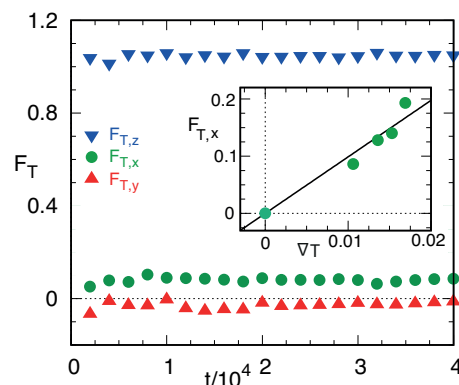


Fig. 3 Thermophoretic force obtained from simulations as a time average for a fixed smooth rod ($l/d = 0.3$), of aspect ratio $L/d = 3.7$, and interaction potential r_6 . The rod is fixed with an angle $\theta = 45^\circ$ with respect to ∇T . The force perpendicular to ∇T , $F_{T,x}$, is non-vanishing as predicted by Eq. (6). The inset shows the value of $F_{T,x}$ for various values of ∇T .

Simulations with single rods fixed by an angle θ with respect to the temperature gradient are performed for different orientations, as shown in Fig. 4. The values of $\alpha_{T,\parallel}$ and $\alpha_{T,\perp}$ can be obtained by fitting the expressions Eqs. (5) and (6) to the simulation results, or more efficiently, just by fixing the rod parallel ($\theta = 0$) or perpendicular ($\theta = \pi/2$) to the temperature gradient. The linear decomposition of the thermophoretic force in Eqs. (5) and (6) is clearly verified by these simulation results.

Results in Fig. 4 also show that, depending on the simulated rods, $F_{T,\parallel}$ can be larger or smaller than $F_{T,\perp}$, such that the force perpendicular to the gradient, $F_{T,x}$, can appear in both directions. This is in strong contrast to the friction force, which is always larger for rods oriented perpendicular to the flow than for those parallel to it. Hence, the anisotropic thermophoretic effect is fundamentally different from the anisotropy of the translational friction.

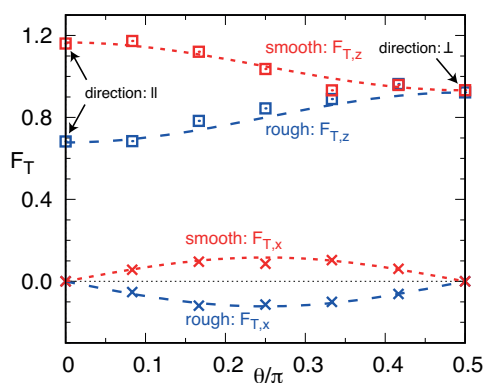


Fig. 4 Thermophoretic force for fixed smooth ($l/d = 0.3$) and rough ($l/d = 0.9$) rods with $L/d = 3.7$ and $r6$. The angle θ denotes the rod orientation with respect to ∇T , as sketched in Fig. 2c. The force $F_{T,z}$ is measured in the direction parallel to ∇T and $F_{T,x}$ perpendicular to it. Symbols correspond to simulation results and lines to the expressions in Eq. (5) and (6).

3.2 Does thermophoretic anisotropy induce orientation?

As just discussed, elongated particles fixed aligned with the temperature gradient or perpendicular to it, can experience well-differentiated thermophoretic forces. Nevertheless, a freely moving rod in a temperature gradient, suffers a force exerted on one half of the rod which is exactly the same as in the other half, such that there is no net torque on the particle. For the same reason, friction forces are also known not to induce any orientation effects on elongated particles, in spite of their anisotropy. Orientation is induced only in the case that the flow field is in itself not homogeneous, as it is the case of a shear flow. The thermophoretic anisotropy does therefore induce no particle alignment. A freely rotating rod in a temperature gradient, will then change its orientation only due to stochastic interactions, being then characterized by a unique thermodiffusion factor, $\alpha_{T,iso}$, which would be determined by the average over all possible rod orientations. Simulations allowing particle rotation limited to two dimensions confirm this statement for the two parameter sets in Fig. 4, and the measured thermodiffusion factors verify that

$$\alpha_{T,iso} = \frac{1}{2} (\alpha_{T,\perp} + \alpha_{T,\parallel}) = \alpha_{T,\parallel} |_{\theta=45}. \quad (7)$$

This can be generalized to rods freely moving in three dimensions as

$$\alpha_{T,iso} = \frac{1}{3} (2\alpha_{T,\perp} + \alpha_{T,\parallel}). \quad (8)$$

While alignment refers to the first moment of the induced orientation, we could wonder if the effect exist in higher moment orders. It is therefore interesting to investigate if the presence of an external temperature gradient could modify the particle rotational diffusion. We measure the rotational diffusion coefficient by characterizing the long time behaviour of the mean squared orientation displacement. For computational efficiency, these simulations consider rods composed of smaller beads, $d = 2a$. The normalizing factor $D_r^0 \simeq 8 \times 10^{-4}$ is obtained for the rough rods in the absence of temperature gradient. In the presence of non-vanishing temperature gradients, simulations are performed by

keeping the rod center of mass fixed in the middle of the simulation box where the solvent average temperature is $k_B \bar{T} = 1$. The simulation data in Fig. 5 show to increase with the applied

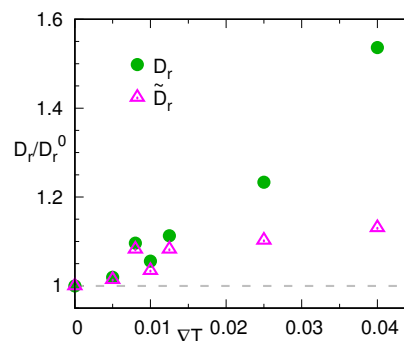


Fig. 5 Normalized diffusion coefficient for a freely rotating rod (with $l/d = 0.3$, $L/d = 3.7$, and $r6$) at various temperature gradients. Bullets correspond to the direct simulation measurements D_r , and triangles to the coefficient rescaled with the density correction \tilde{D}_r .

temperature, but this is mainly due to the particular equation of state of the employed MPC fluid, which is that of an ideal gas. Given a spatial linear increase of the temperature, the related position dependent density will be only approximately linear⁴⁴. The density in the middle of the simulation box will then differ from the average one, which will affect the rotational diffusion coefficient. If we consider that $D_r \propto 1/\eta$, and that $\eta \propto (\rho - 1)^{54}$ we can explain the major D_r by considering the rescaled coefficient $\tilde{D}_r = D_r(\rho|_{L_z/2} - 1)/(\rho - 1)$. The factor $\rho|_{L_z/2}$ can be measured in the simulations, or calculated from the ideal gas equation of state as $\rho/\rho|_{L_z/2} = \bar{T} \ln(T_h/T_c)/(T_h - T_c)$ ⁴⁴. The rescaled coefficient \tilde{D}_r in Fig. 5 shows to be mostly independent of the applied temperature gradient within the precision of the data, which demonstrates that the temperature gradient has no effect in the particle orientation.

It is interesting to mention that *thermomolecular orientation* has been previously reported in diatomic fluids^{55–57}. In these cases, elongated molecules made of two atoms with unequal sizes show to display certain average orientation towards the direction of the temperature gradient. This does not contradict the discussed lack of orientation induced by anisotropic thermophoresis, since the particles we discuss are elongated but intrinsically symmetric, namely composed of indistinguishable building blocks.

3.3 Aspect ratio effect

For spherical colloids, the size is well-known to influence α_T , the particle thermodiffusion factor^{47,58,59}. The overall increase of size of the rod will therefore also translate into an increase of α_T , but how does the rod aspect ratio influence the anisotropic effect, still needs to be clarified.

Simulations of rods with orientations parallel and perpendicular to the temperature gradient are performed for different aspect ratios and for two rugosities as shown in Fig. 6 and Fig. 7. In order to compare with two different experimental approaches, we change the rod aspect ratio following two different strategies. The first strategy consists in fixing the particle diameter and changing

its length. This is the case of polymeric rods made out of different number of monomers. We simply simulate rods with various numbers of adjacent beads, results are shown in Fig. 6. Obtained

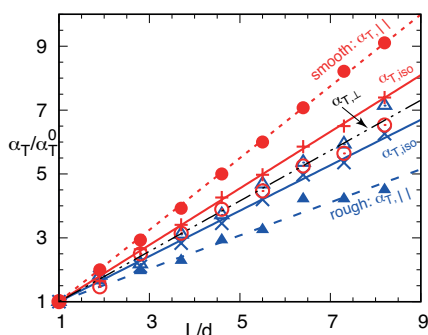


Fig. 6 Normalized thermodiffusion factors for rods of fixed diameter d and varying length L . Parallel (open symbols), perpendicular (filled symbols), and freely rotating (crosses, calculated from Eq. (8)) thermodiffusion factors are presented together with linear fits. Results are presented for both smooth and rough rods (rugosity parameters $l/d = 0.3$ and 0.9) with $r6$ interaction potential.

measurements are normalized with α_T^0 , the thermal diffusion factor of a single bead of the same characteristics as the ones employed to build the rod, such that for $L = d$, $\alpha_{T,\perp} = \alpha_{T,\parallel} = \alpha_T^0$ by definition. The four analyzed cases in Fig. 6 show a very clear linear increase of α_T with the aspect ratio L/d , although with different slopes. This linear increase means that by characterizing the values of α_T at two different aspect ratios with enough precision, would allow us to easily extrapolate to other aspect ratios; also in the case that one of those values is the limiting spherical case α_T^0 .

Interestingly, in the case of a freely rotating colloidal rod, the overall thermodiffusion factor also increases linearly with the aspect ratio of the colloidal rod, given the verified expression in Eq. (7) and Eq. (8). This is very interesting by itself, and reminiscent of the well-known effect of the particle moment of inertia on the thermal diffusion in molecular mixtures^{6–8}. The linear increase agrees with the theoretical expression in Ref.¹⁰ in the case of very thin double layer. The increase is also consistent with the experimental results in Ref.⁶⁰ for double and single strained DNA with two different number of monomers.

The second strategy to investigate the effect of the aspect ratio consists in keeping the colloid surface area constant, such that the increasing the length is accompanied by a decrease of the particle diameter. This can correspond to deformable structures such as vesicles, droplets, or polymeric globules⁶⁰. In order to keep similar thermophoretic effect per unit area^{47,61}, we maintain the interaction range constant for increasing bead size by making use of the displaced potential in Eq. (1). We fixed $d = 4$ and increase Δ such that the effective bead diameter is $d_{ef} = d + 2\Delta$. We approximate the surface of simulated shish-kebab rod in Fig. 1, by that of a spherocylinder such that $S = \pi d_{ef} L$, quantity that we keep then constant together with the rod rugosity. We take as reference the rod simulated in Fig. 6 with $L/d = 6.4$, then we decrease the number of beads by increasing the rod thickness by increasing Δ . Figure 7 shows that in this case all thermophoretic factors

decrease in magnitude with aspect ratio L/d_{ef} which agrees with the theoretical expression in Ref.⁶⁰.

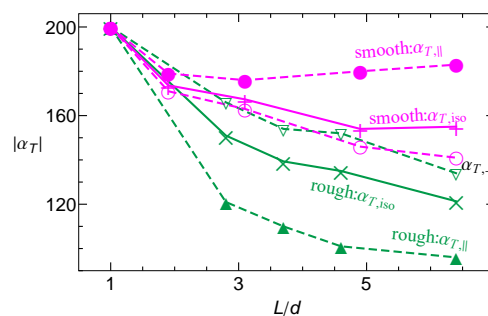


Fig. 7 Thermodiffusion factors for rods of fixed surface S . Symbols, potential, and rugosity parameters are similar to Fig. 6. Lines connect symbols as guide to the eye.

To understand the linear increase of $\alpha_{T,\perp}$ and $\alpha_{T,\parallel}$ with L for fixed d , we can employ a geometrical argument by approximating the rod to an elongated parallelepiped of dimensions $d \times d \times L$. The surface aligned with the temperature gradient for a rod aligned with the gradient is $4dL$, while for a rod perpendicular to the gradient this surface is $2dL + 2d^2$, both increasing with L . Then, if we assume that each α_T is directly proportional to the surface aligned with the temperature gradient, the effect would be explained. Similar reasoning for the case of fixed S would predict an increasing $\alpha_{T,\parallel}$, and decreasing both $\alpha_{T,\perp}$, and $\alpha_{T,iso}$. This is still very reasonable, since the assumed direct proportionality of the surface and the thermophoretic force is not necessarily precise; as well as the contribution of the balance of the two surfaces at constant temperature might not be negligible.

3.4 Surface effects

The rod surface is modified in our model in two different manners. On the one hand, the surface shape as described in Fig. 1 modifies its rugosity with the parameter l/d . On the other hand, the choice of the employed potential, attractive-repulsive, soft-steep will also modify the thermophoretic properties of the rod. To analyze more in detail these effects, further simulations calculate $\alpha_{T,\parallel}$ and $\alpha_{T,\perp}$ as a function of the different potential interactions and the rugosity parameter l/d , as shown in Fig. 8 and Fig. 9. In the case of spherical colloids, the thermodiffusion factor α_T^0 is known to depend on the colloid-surface interactions, and on the colloid size^{4,47}. With rods of fixed aspect ratio, we perform simulations with repulsive and attractive potentials, and with different n values in Eq. (1), for which α_T^0 is also evaluated. The parallel $\alpha_{T,\parallel}$, and perpendicular $\alpha_{T,\perp}$, thermodiffusion factors are compared with α_T^0 , as displayed in Fig. 8. Values larger than the reference linear increase in Fig. 8, in absolute numbers, indicate the enhancement of the thermal diffusion factors due to the increase elongation of the rod. This enhancement is clear in all investigated cases, although its magnitude differs for the different potentials, rugosities, and orientations. In general, the increase of $\alpha_{T,\parallel}$ and $\alpha_{T,\perp}$ shows to be larger, the larger the α_T^0 .

The effect of the surface rugosity can already be observed

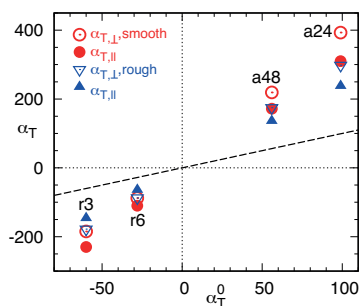


Fig. 8 Parallel and perpendicular thermodiffusion factors for rods with $L/d = 3.7$ with various interaction potentials (indicated in the labels) as a function of α_T^0 , the thermodiffusion factor of a single bead. Results are provided for the same two rugosity parameters as in Fig. 6. The dashed line is a guide to the eye.

in Fig. 4 and Fig. 6 where simulation results of two well-differentiated rod rugosities are presented. For the repulsive potential and aspect ratio here employed, the rough rod shows $|\alpha_{T,\parallel}| < |\alpha_{T,\perp}|$; *i. e.* the thermophoretic force for the rod aligned with the temperature gradient is smaller than for the perpendicular one. Meanwhile the smooth rod with the same potential shows the opposite behavior, $|\alpha_{T,\parallel}| > |\alpha_{T,\perp}|$. This means that by changing the rugosity of the rod, the forces perpendicular to the temperature gradient can invert their direction, as shown in Fig. 4. This is though not the case for the rods simulated with attractive interactions where $\alpha_{T,\parallel} < \alpha_{T,\perp}$ for both the smooth and the rough surfaces. Note that the sign of the thermodiffusive factors is never modified, such that the thermophilic/thermophobic character of the colloids does not change with its shape change from spherical into elongated, and it will be therefore the same for both components $\alpha_{T,\parallel}$ and $\alpha_{T,\perp}$.

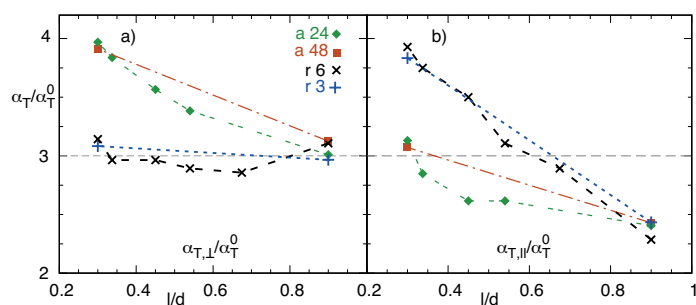


Fig. 9 Normalized parallel and perpendicular thermodiffusion factors for rods with $L/d = 3.7$ as a function of the rugosity parameter l/d . Simulations with various interaction potentials are reported and indicated in the corresponding labels. The horizontal line is a guide to the eye.

The dependence of the thermal diffusion factors with the rugosity parameter l/d , is shown in Fig. 9. With increasing rugosity of the rod surface, the thermal diffusion factor shows to decrease, or to remain unchanged. In other words, smoother surfaces produce larger thermophoretic responses or eventually similar than their rough counterparts. The clear decrease of $\alpha_{T,\parallel}$ with increasing rugosity is what eventually changes the relative importance of both factors and the direction of the force perpendicular to the

temperature gradient.

To explain these dependencies, we should discuss two types of contributions, which are again related to the rod-solvent interaction potentials and the surface shape. The finite range of the solvent-bead interactions results in overlapping regions, in which solvent particles can simultaneously interact with more than one neighboring bead. The size of these overlapping areas decreases with increasing roughness, or potential steepness, modifying the effective rod-solvent potential. This effect is smaller for rough rods, for which the thermodiffusion factors in Fig. 9 have little dependence of the type of potential. Smooth rods interestingly show a difference between attractive (thermophobic) potentials, and repulsive (thermophilic) ones, but not between those with different steepness. The second type of contribution is in this case dominant, and related to the surface shape, and in particular with the presence of surface indentations which can explain the decrease of $\alpha_{T,\parallel}$ with increasing roughness. To estimate the contribution to thermophoretic force between two arbitrary points at the rod surface, we consider first that the thermophoretic factor along a wall, can be assumed to be directly proportional to the wall length, which has been shown in Fig. 6. By considering Eq. (2), and that the gradient depends on the inverse of the distance, the contribution to thermophoretic force can then be determined by the difference of temperatures between these two points T_c and T_h . Figure 10 illustrates the thermophoretic forces along a wall with an indentation, F_A , and a flat wall F_B , which are both considered to be the sum of two contributions by considering the temperature at the middle of the wall T_m . Indented and flat walls have different lengths, but the temperatures at their ends are the same. The wall length increase exactly cancels with the decrease of the temperature gradient, such that the wall thermophoretic forces are precisely the same, this is $F_{A1} = F_{B1}$ and $F_{A2} = F_{B2}$. The total force in both cases is though not the same due to the angle θ that determines the indentation, as sketched in Fig. 10, such that the force in the indented surface F_A is a factor $\cos\theta$ smaller than the force in the perfectly smooth surface $F_B = F_A/\cos\theta$. This effect is very clear when the rod is aligned

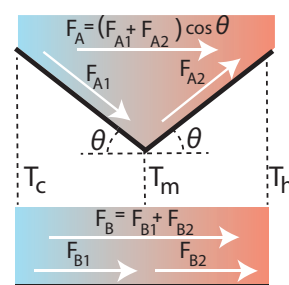


Fig. 10 Sketch illustrating the decrease of the thermophoretic force along an indented surface.

with the temperature gradient, and explains the clear decrease of $\alpha_{T,\parallel}$ with l/d for all potentials in Fig. 9b. When the rod is perpendicular to the gradient, the effect of the indentation is subtly different but still present due to employed three-dimensional structure. However, the overall contribution is smaller which explains the unchanged or decreasing dependence of $\alpha_{T,\perp}$ with l/d

in Fig. 9a.

3.5 Thermophoretic anisotropy factor

The importance of the anisotropic effect is determined by how different are the thermophoretic forces of the rods aligned and perpendicular to the temperature gradient. We therefore define the dimensionless *thermophoretic anisotropy factor* as

$$\chi_T = \alpha_{T,\perp} - \alpha_{T,\parallel}. \quad (9)$$

The intensity and the sign of the force perpendicular to the temperature gradient is simply determined by χ_T , as already shown in Eq. (6). The direction of the perpendicular force will have crucial importance in applications of the effect, determining for example the rotation direction of the thermophoretic turbines¹⁴. This means that the sign of α_T^0 will not be enough to know the direction of the perpendicular force; or, in other words, the thermophilic or thermophobic character of the surface does not determine the direction of the transverse phoretic effect.

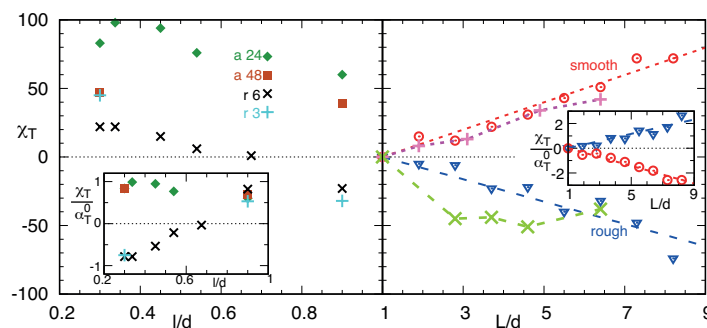


Fig. 11 a) Asymmetric thermophoretic factor χ_T as function of the rod rugosity parameter, for various interaction potentials, with $L/d = 3.7$ from the data in Fig. 9. b) χ_T as a function of the aspect ratio for $r=6$ interaction potential and rugosities $L/d = 0.3$ and 0.9 . Circles and triangles correspond to the data in Fig. 6 for rods of fixed diameter. The insets correspond to the ratio χ_T/α_T^0 for the same data. Pluses and crosses correspond to the data in Fig. 7 for rods of fixed surface.

The value of χ_T is displayed for various potentials and rugosities in Fig. 11, where it can be observed that $\chi_T > 0$ in the majority of the cases. This means that the perpendicular force happens most of the time in the same direction, which is positive with the convection in Fig. 2. In the thermophobic case, where the thermodiffusion factor is positive, $\chi_T > 0$ corresponds to $|\alpha_{T,\perp}| > |\alpha_{T,\parallel}|$. This resembles the well-known translational friction case and provides the opposite trend as the predictions for aerosols^{15,16}, showing to be an effect specific of colloids in solution. On the other hand, in the thermophilic case, where the thermodiffusion factors are negative, $\chi_T > 0$ corresponds to $|\alpha_{T,\perp}| < |\alpha_{T,\parallel}|$. For comparison, the insets in Fig. 11 show the ratio χ_T/α_T^0 , which will be positive in the friction-like cases, and negative otherwise. This normalization also provides a rapid estimation of the magnitude of the effect which can be as expected to be as large as the phoretic effect itself, even for the small aspect ratios here considered. Note though that these are the results obtained by means of computer simulation and that in practical experiments, the results can show a much richer behavior. With

our simulation results, we observe that by changing the surface rugosity, the anisotropic effect can reverse its direction in the case of thermophilic rods. We expect this behavior to be reproducible experimentally by changing the surface coating, electrostatic interactions, average temperature, or any of the factors that are known to affect the thermophoretic behavior.

4 Conclusions

Anisotropic thermophoresis refers to the different phoretic thrust that an elongated particle suffers when aligned with the temperature gradient and when perpendicular to it. This difference results in a contribution to the thermophoretic force perpendicular to the temperature gradient when the rod is fixed oblique to the gradient. This anisotropy does not have any relevant effect on the particle orientation, nor on the rotational diffusion of the particle, given the considered symmetry of the colloidal rod. The existence of anisotropic thermophoresis is relatively intuitive, especially by comparing with the translational friction of a rod which is also noticeable different if aligned with the flow, or perpendicular to it. Here we analyze this effect in detail, showing that the intensity and the direction of the force is a function of the aspect ratio, the surface geometry, and the colloid-fluid interactions. Increasing aspect ratio by fixing the particle radius, increases the anisotropic phoretic effect in a straightforward manner. The rugosity of the colloidal surface is also relevant, being smooth surfaces the ones with larger anisotropic thermophoretic effect. In general, surfaces with larger phoretic effect also have larger anisotropic phoretic effect. Interestingly, for the simulation potentials employed in this work, the direction of the phoretic force perpendicular to the gradient is the same for both thermophobic and thermophilic colloids. Only rods with thermophilic and rough surface have shown in our simulations to display the perpendicular forces with opposite direction. We expect that experimental results will show an even richer behavior, in which the intensity and the direction of the effect could depend on many factors such as intrinsic surface properties, eventual coatings, average fluid temperature and density, presence of salt ions, and various other factors. Note that since our simulation model does not include any of these aspects, only qualitative trends can be predicted. For example, the model has already been able to explain the experimentally observed dependence of the isotropic thermophoretic factor with the rod aspect ratio, with two types of constraints⁶⁰. Two first practical applications of anisotropic thermophoresis have already been proposed for the construction of phoretic microturbines and micropumps. In the presence of external temperature gradients, the blades of a microturbine will rotate when being anisotropic¹⁴, and a microchannel will experience some spontaneous directed fluid motion when including elongated tilted obstacles⁶².

Although the work presented here has been exclusively focused in the thermophoretic effect, very similar results are expected with other phoretic effect such as diffusiophoresis. A direct proof for this is the fact that a similar micro-turbine placed in an external concentration gradient has shown to display similar behavior due to the related anisotropic diffusiophoresis⁶³. In summary, with this investigation, we provide a deep insight into the anisotropic thermophoresis of elongated micro-meter size objects;

effect that we hope will be soon experimentally verified, and find applications in different fields like particle characterization, microfluidics, or biomedicine.

Acknowledgments

We thank helpful discussions with Adam Wysocki and Jinglei Hu. The authors acknowledge financial support by China Scholarship Council (CSC), and by the Bavarian Ministry of Economic Affairs and Media, Energy and Technology within the joint projects in the framework of the Helmholtz Institute Erlangen-Nürnberg for Renewable Energy (IEK-11) of Forschungszentrum Jülich. We also gratefully thank the computing time granted on the supercomputer JURECA at Jülich Supercomputing Centre (JSC). M. Y. also acknowledges financial support of the NSFC (No. 11674365).

References

- C. Ludwig, Sitzungsber. Preuss. Akad. Wiss., Phys. Math. Kl. **20**, 539 (1856).
- C. Soret, Arch. Sci. Phys. Nat. **3**, 48 (1879).
- S. Wiegand, J. Phys.: Condens. Matter **16**, R357 (2004).
- R. Piazza and A. Parola, J. Phys.: Condens. Matter **20**, 153102 (2008).
- A. Würger, Rep. Prog. Phys. **73**, 126601 (2010).
- D. Reith and F. Müller-Plathe, J. Chem. Phys. **112**, 2436 (2000).
- C. Debuschewitz and W. Köhler, Phys. Rev. Lett. **87**, 055901 (2001).
- G. Galliéro, B. Duguay, J.-P. Caltagirone, and F. Montel, Fluid Phase Equilibria **208**, 171 (2003).
- P. Blanco, H. Kriegs, M. P. Lettinga, P. Holmqvist, and S. Wiegand, Biomacromolecules **12**, 1602 (2011).
- Z. Wang, H. Kriegs, J. B. J. K. G. Dhont, and S. Wiegand, Soft Matter **9**, 8697 (2013).
- S. Duhr and D. Braun, Phys. Rev. Lett. **96**, 168301 (2006).
- S. Iacopini, R. Rusconi, and R. Piazza, Eur. Phys. J. E **19**, 59 (2006).
- M. Doi and S. F. Edwards, *The Theory of Polymer Dynamics* (Oxford University Press, Oxford, 1986).
- M. Yang, R. Liu, M. Ripoll, and K. Chen, Nanoscale **6**, 13550 (2014).
- P. Garcia-Ybarra and D. E. Rosner, AIChE Journal **35**, 139 (1989).
- F. Zheng, Adv. Colloid Interface Sci. **97**, 253 (2002).
- K. Ghorayeb, A. Firoozabadi, and T. Anraku, SPE Journal **18**, 114 (2003).
- J. Giddings, Science **260**, 1456 (1993).
- P. Baaske, F. M. Weinert, S. Duhr, K. H. Lemke, M. J. Russell, and D. Braun, Proc. Natl. Acad. Sci. **104**, 9346 (2007).
- D. Niether, D. Afanasenkau, J. K. G. Dhont, and S. Wiegand, Proc. Natl. Acad. Sci. **113**, 4272 (2016).
- M. Jerabek-Willemsen, T. André, R. Wanner, H. M. Roth, S. Duhr, P. Baaske, and D. Breitsprecher, J. Mol. Struct. **1077**, 101 (2014).
- D. Vigolo, R. Rusconi, H. A. Stone, and R. Piazza, Soft Matter **6**, 3489 (2010).
- M. Yang and M. Ripoll, Soft Matter **12**, 8564 (2016).
- H. R. Jiang, N. Yoshinaga, and M. Sano, Phys. Rev. Lett. **105**, 268302 (2010).
- M. Yang and M. Ripoll, Phys. Rev. E **84**, 061401 (2011).
- M. Yang, A. Wysocki, and M. Ripoll, Soft Matter **10**, 6208 (2014).
- A. Malevanets and R. Kapral, J. Chem. Phys. **110**, 8605 (1999).
- A. Malevanets and R. Kapral, J. Chem. Phys. **112**, 7260 (2000).
- R. Kapral, Adv. Chem. Phys. **140**, 89 (2008).
- T. Ihle and D. M. Kroll, Phys. Rev. E **63**, 020201(R) (2001).
- M. Ripoll, K. Mussawisade, R. G. Winkler, and G. Gompper, Phys. Rev. E **72**, 016701 (2005).
- E. Tüzel, T. Ihle, and D. M. Kroll, Phys. Rev. E **74**, 056702 (2006).
- I. O. Götze, H. Noguchi, and G. Gompper, Phys. Rev. E **76**, 046705 (2007).
- H. Noguchi, N. Kikuchi, and G. Gompper, Europhys. Lett. **78**, 10005 (2007).
- M. Yang, M. Theers, J. Hu, G. Gompper, R. G. Winkler, and M. Ripoll, Phys. Rev. E **92**, 013301 (2015).
- N. Kikuchi, C. M. Pooley, J. F. Ryder, and J. M. Yeomans, J. Chem. Phys. **119**, 6388 (2003).
- C. M. Pooley and J. M. Yeomans, J. Phys. Chem. B **109**, 6505 (2005).
- T. Ihle, E. Tüzel, and D. M. Kroll, Phys. Rev. E **72**, 046707 (2005).
- H. Noguchi, N. Kikuchi, and G. Gompper, Europhys. Lett. **79**, 36002 (2007).
- R. G. Winkler and C.-C. Huang, J. Chem. Phys. **130**, 074907 (2009).
- C. Huang, A. Varghese, G. Gompper, and R. Winkler, Phys. Rev. E **91**, 013310 (2015).
- K. Mussawisade, M. Ripoll, R. G. Winkler, and G. Gompper, J. Chem. Phys. **123**, 144905 (2005).
- M. Yang and M. Ripoll, Soft Matter **9**, 4661 (2013).
- D. Lüsebrink and M. Ripoll, J. Chem. Phys. **136**, 084106 (2012).
- F. Müller-Plathe, J. Chem. Phys. **106**, 6082 (1997).
- G. A. Vliegenthart, J. F. M. Lodge, and H. N. W. Lekkerkerker, Physica A **263**, 378 (1999).
- D. Lüsebrink, M. Yang, and M. Ripoll, J. Phys.: Condens. Matter **24**, 284132 (2012).
- M. P. Allen and D. J. Tildesley, *Computer Simulations in Liquids* (Clarendon, Oxford, 1987).
- A. Parola and R. Piazza, J. Phys.: Condens. Matter **17**, S3639 (2005).
- M. Yang and M. Ripoll, J. Phys.: Condens. Matter **24**, 195101 (2012).
- M. Yang and M. Ripoll, J. Chem. Phys. **136**, 204508 (2012).
- H. R. Jiang, H. Wada, N. Yoshinaga, and M. Sano, Phys. Rev.

- Lett. **102**, 208301 (2009).
- 53 L. Helden, R. Eichhorn, and C. Bechinger, *Soft Matter* **11**, 2379 (2015).
- 54 T. Ihle and D. M. Kroll, *Phys. Rev. E* **67**, 066706 (2003).
- 55 F. Römer, F. Bresme, J. Muscatello, D. Bedeaux, and J. M. Rubí, *Phys. Rev. Lett.* **108**, 105901 (2012).
- 56 C. D. Daub, P.-O. ØAstranda, and F. Bresme, *Phys. Chem. Chem. Phys.* **16**, 22097 (2014).
- 57 A. A. Lee, *Soft Matter* **12**, 8661 (2016).
- 58 M. Braibanti, D. Vigolo, and R. Piazza, *Phys. Rev. Lett.* **100**, 108303 (2008).
- 59 S. Duhr and D. Braun, *Proc. Natl. Acad. Sci.* **103**, 19678 (2006).
- 60 M. Reichl, M. Herzog, F. Greiss, M. Wolff, and D. Braun, *Phys. Rev. E* **91**, 062709 (2015).
- 61 D. Lüsebrink, Ph.D. thesis, Cologne University, Cologne, Germany (2011).
- 62 Z. Tan, M. Yang, and M. Ripoll, *Microfluidic pump by anisotropic thermophoresis*, (preprint, 2017).
- 63 M. Yang, R. Liu, M. Ripoll, and K. Chen, *Lab Chip* **15**, 3912 (2015).